UNIVERSITY of CALIFORNIA
SANTA CRUZ

EXAMINING THE SELF INTERACTION OF DARK MATTER THROUGH BRIGHTEST CLUSTER GALAXY OFFSETS

A thesis submitted in partial satisfaction of the
requirements for the degree of

BACHELOR OF SCIENCE

in

PHYSICS

by

Dane Cross

10 June 2020

Abstract

Examining the Self Interaction of Dark Matter through Brightest Cluster Galaxy Offsets

by

Dane Cross

Dark matter makes up 5/6 of the matter in the universe, but we do not know some of its most basic characteristics. In this thesis, I find evidence that is consistent with the Self Interacting Dark Matter (SIDM) model, which predicts that dark matter interacts with itself in much the same way that the matter we see around us interacts with itself. In order to test SIDM, I use observations of galaxy clusters, which have dense cores of dark matter at their centers. Simulations show that if dark matter interacts with itself, then the Brightest Cluster Galaxy (BCG) in each cluster will tend to be offset from the center of mass of the dark matter core. I determined the centers of mass of the dark matter cores by taking the centroids of the x-ray signature of the luminous gas in gravitational equilibrium with the dark matter core. I measured the errors on these centroids by making noise simulations of the x-ray data and remeasuring the centroid.

These measurements show that in relaxed clusters, the typical BCG/x-ray centroid offset is 12.30 ± 0.72 kilo-parsecs (kpc) for the 14 clusters I examined. If I place more stringent guidelines on the relaxation of the clusters, that measured offset becomes 1019 ± 1.77 kpc. This offset is larger than zero to a statistically significant degree, and thus this result is consistent with the existence of self interacting dark matter.

Contents

1

Introduction

Dark matter makes up 5/6 of the matter in the universe, but since it does not interact with photons, there is no way for us to directly observe it (Zwicky, 1933; Rubin & Ford, 1970). Since its discovery, scientists have been trying to understand the nature of this substance through indirect observation, but there are currently too many models which fit the observed data.

An example of one of these models is the Cold Dark Matter (CDM) model, which predicts that dark matter became non-relativistic very early after the big bang (Davis et al., 1985). Therefore the particles were not transported evenly throughout the universe, but instead stayed gravitationally bound to each other in high density regions. Using this model, scientists have generated promising simulations of the formation of the universe (Davis et al., 1985; Anderson et al., 2014; Percival et al., 2001; de la Torre et al., 2013).

One notable simulation was published by Springel et al. (2005) called the "Millennium Simulation," which was one of the first simulations to recreate the formation of galaxy clusters in the large scale universe. This simulation also exhibited the dark matter halos that we see surrounding luminous galaxies. These halos are smaller concentrations of dark matter inside of the cluster, as illustrated by the small bright spots in Figure 1.1.

One important feature of CDM theory is that the CDM model predicts a sharply concentrated

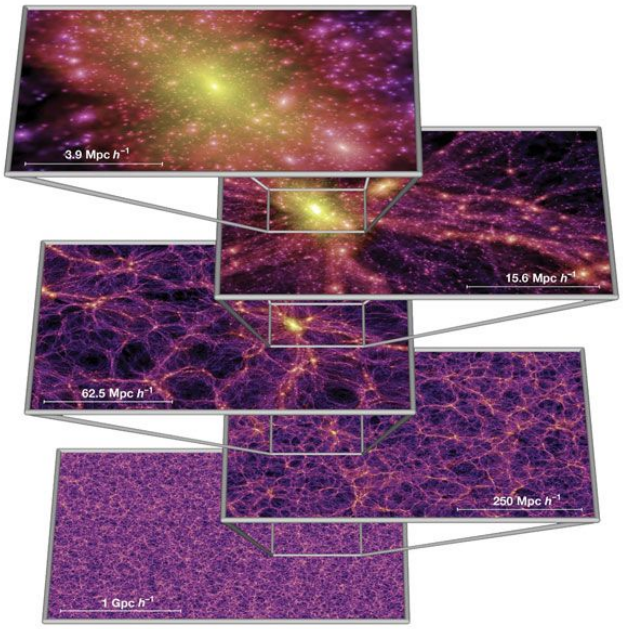

Figure 1.1: Millennium Simulation results exhibiting the projected density of dark matter in the universe. The brighter colors represent a higher dark matter density, while darker colors represent lower density areas, where the color scale goes yellow to magenta to black. The top image shows the simulation on the scale of a galaxy cluster. The density distributions for each bright spot of dark matter have a very sharp density profile. Some of these bright spots are home to galaxies of luminous matter. For successively lower images, the frame is zoomed out. The second, third, and fourth picture show that the galaxy cluster from the first image sits on a high density node in a web-like structure. From Springel et al. (2005)

dark matter halo in the center of galaxies. This occurs because the only force accounted for in the CDM model is gravity, so there is no force that can resist the gravitational collapse of such halos. This would result in a sharp, centrally concentrated "cuspy" density distribution.

Despite the successes of the CDM model, we know that a "cuspy" dark matter distribution is not supported by observations. According to observations from Casertano & van Gorkom (1991) and Flores et al. (1993), the real velocity distributions of matter in galaxies is much lower than the velocity distributions predicted by CDM. In other words, if real spiral galaxies rotated at the rate predicted by the CDM model, then those galaxies would become unbound. Galactic orbits are larger and slower than expected by the CDM model, which means that the mass distribution in the center of galaxies predicted by the CDM model is too cuspy (Dubinski & Carlberg, 1991).

This cuspy distribution problem can be solved if we alter the CDM model to allow for self-

interaction between dark matter particles. If there is some force resisting gravitational collapse, then dark matter halos would have a shallower, wider density profile. This would lessen the gravitational pull experienced by galactic objects because there will be less mass concentrated at the center of the galaxy. This would allow objects to orbit at larger radii and lower velocities, aligning more closely to observational data. Physicists have dubbed this correction to the CDM model the Self-Interacting Dark Matter (SIDM) model (Spergel & Steinhardt, 2000).

In this thesis, I will test the SIDM correction to CDM model. Specifically, I will be finding observational proof that determines if the distribution of dark matter concentrations are "cuspy" or more spread out. My laboratory will be the massive dark matter cores which bind galaxies into clusters.

In order to determine the dark matter distribution in these galaxy clusters, scientists look to x-ray astronomy. The gravity associated with the dark matter cores accelerates the gas of the IntraCluster Medium (ICM) towards high density regions of dark matter. This gravitational collapse leads to an increase in temperature high enough to ionize the ICM. The temperatures of these ionized gasses lead to acceleration of electrons which is high enough to trigger Bremsstrahlung radiation with energies in x-ray. Accordingly, observing x-ray density in a galaxy cluster gives a rough indication of where the dark matter is concentrated (Delliou et al., 2019).

The location of dark matter cannot be directly determined by looking to x-ray emissions from any galaxy cluster. This is because the x-ray source is the ICM, which is luminous matter and therefore most likely interacts with itself differently than dark matter interacts with itself. Thus, the shape of the x-ray emissions will not directly reflect the shape of the dark matter distribution. This is why we do not rely on the shape of the x-ray distribution to determine the dark matter density profile. Instead, I examine the x-ray centroid of a relaxed cluster[1] because in a relaxed cluster, the dominant force on the gas will be gravity. With this information, we can examine how this center of mass relates to the

[1] A relaxed galaxy cluster is defined in much the same way that a relaxed spring is defined. The cluster could have undergone some displacement in the past (for example a collision with another cluster), but non-conservative forces have taken away energy from the oscillations until the cluster relaxes to equilibrium. In this relaxed state, the density of the cluster will be spherically symmetric. There will be more on why we need relaxed clusters in the Methodology section.

luminous matter around it.

In this thesis, I will compare the dark matter center of mass to the Brightest Cluster Galaxy (BCG). BCGs form near the center of dark matter nodes, which serves as a deep gravitational well to which massive objects (such as other galaxies) are attracted. This makes BCGs the brightest and heaviest galaxies in their respective clusters (Lin & Mohr, 2004). If this dark matter center is cuspy, then the BCG will tend to be exactly on the center of the dark matter distribution. If the dark matter core has a flatter profile, then the BCG will tend to be offset from the center (Kim et al., 2016).

This offset occurs because galaxy clusters are constantly moving and colliding with each other. BCGs do not experience any strong damping force, and the SIDM model predicts a flatter dark matter distribution (Read et al., 2006). This means that BCGs in the SIDM model are less bound to the dark matter centers of mass. On the other hand, if dark matter does not interact with itself, as in CDM, the dark matter cores would have a sharper matter distribution. This would mean that galaxy clusters can merge and relax while keeping their BCGs tightly bound to their centers (Markevitch et al., 2004).

If we can observe BCG offsets, they would tell us that dark matter exhibits a wider, flatter distribution. Observing this phenomenon could place the most stringent constraints on dark matter collisionality yet observed (Kim et al., 2016).

For the remainder of the introduction, I will be going into more depth on the theory and significance of CDM and SIDM. Then, in the methodology section, I will discuss in further detail the data we selected and the method for determining the center of the x-ray distribution. In the results section, I will outline the information that we found, and in discussion section, I will state what the results mean for the future of dark matter research.

1.1 Cold Dark Matter and the Formation of the Universe

Cosmology, a sub-field in astrophysics that studies the origin of the universe, relies heavily on understanding the fundamental particles that make up matter and energy. Scientists think that after

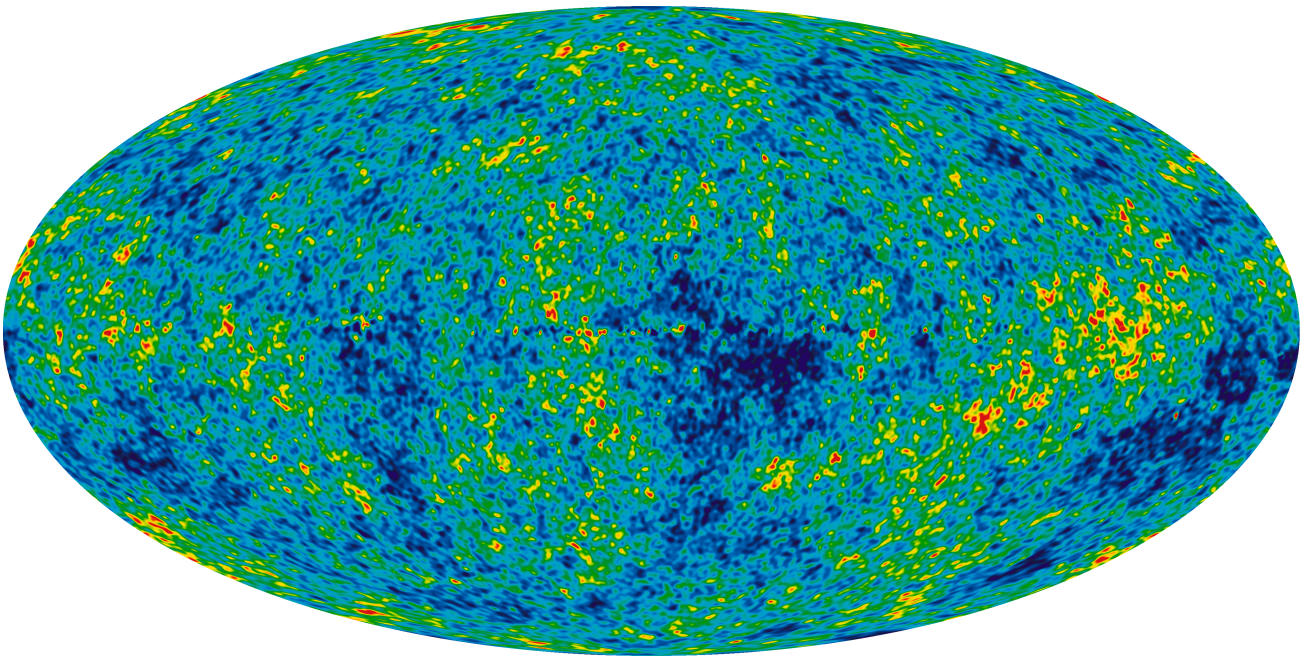

Figure 1.2: Cosmic Microwave Background (CMB). The change in colors represent the colder or hotter spots in the universe, where dark blue represents the area with the lowest temperatures and the red represents the area with the highest temperatures. These perturbations are believed to be the seeds of large scale structure in the universe, places where matter would soon gather and form the node-like, dark matter structure that we see today. Image from NASA & WMAP (2012).

the Big Bang there was a period of inflation, which was characterized by an exponential expansion of the size of the universe (Martin et al., 2013). Because this expansion was so fast and energetic, when slight perturbations in the density of matter and energy occurred at the beginning of inflation, those over-densities were separated very quickly. They were separated so quickly that the matter didn't have time to re-homogenize, and therefore matter after inflation clumped together. These clumps formed the seeds of large scale structure as we see it today (Gott & Rees, 1975). Figure 1.2 illustrates the perturbations that occurred after inflation as we observe them from the Cosmic Microwave Background (CMB) (White et al., 1994). The mechanisms by which matter in this era was formed and interacted with itself determines how often these perturbations occurred and how they stayed as a coherent clump during the violent age of inflation.

Inflation bridged the gap between two ages: the radiation dominated and the matter dominated epoch. The radiation dominated epoch was characterized by photons being the dominant form

of energy in the universe (Martin et al., 2013). After inflation, there was a point where the density of photons decreased enough to allow energy to exist as matter, after which the period of matter domination began (Perkins, 2009). Since the abundance of dark matter is about an order of magnitude higher than the abundance of luminous matter, the matter dominated epoch was really dominated by dark matter (Faber & Gallagher, 1979; Yang et al., 1984). The evolution of the universe during this transition and beyond, accordingly, was heavily influenced by the behaviors of dark matter. The prevailing theory for modelling these behaviors is the CDM model.

CDM is "cold" because in the transition from radiation domination to matter domination, CDM particles became non-relativistic very early (Davis et al., 1985). By definition, the distance a CDM particle travelled before slowing down enough to become gravitationally bound to some structure was on the order of the size of a galaxy. Simulations show that using this model of dark matter creates accurate models of the dark matter web structure found in the universe today (Springel et al., 2005; Davis et al., 1985; Anderson et al., 2014; Percival et al., 2001; de la Torre et al., 2013).

The accuracy of these CDM simulations is promising because this model is relatively simple; it assumes no interaction between dark matter particles. If we were to model luminous matter in such a way, we would be assuming that gravity is the only force, therefore overlooking electromagnetic, strong, and weak interactions. In this regime, large scale structure such as galaxy clusters would be accurately recreated, but there would be differences in smaller scale structures of the universe. For example if these forces did not exist, the chemical reaction that enables fusion in stars would not occur, and instead what we would see is black holes where the stars should be. This would lead to stars having a "cuspy" density profile instead of the flatter density profile that gives stars their dimensions.

Something very similar happens when we assume dark matter doesn't interact with itself. The collisionless CDM model predicts that dark matter halos will have a sharply centralized, "cuspy" density distribution (Flores & Primack, 1994). This cuspy distribution occurs because there is no force that can counteract gravitational collapse. If there was a force that could counteract gravitational

collapse, halos would have a flatter density profile, in the same way that stars which undergo fusion have a flatter density profile.

1.2 Self-Interacting Dark Matter

In order to fix the issues with CDM, many scientists have proposed a regime where dark matter interacts with itself (Carlson et al., 1992). In order to quantify matter interactions, we define the cross section. A cross section is a quantitative number that depicts the probability of two particles interacting. The cross section has units of area; if the particle's cross section is high, its effective surface area is high, and it is more likely that the two particles would interact. For forces that act at a distance, like gravity and electromagnetism, cross sections tend to be larger because the two particles do not need to be physically near each other in order to interact. When discussing the cross sections of dark matter, the units are typically units of area per mass, as we do not know the individual masses of each dark matter particle, just the total mass of dark matter in the universe.

Kim et al. (2016) show that the SIDM model predicts that the dark matter cross section must have an upper limit of 1 cm^2/g. To put this in perspective, the cross section for the annihilation of an electron and positron is (Gordon & Breach, 1967)

$$\sigma_{e^-e^+} = \frac{86.8nb}{m_{e^+} + m_{e^-}}$$

where m_{e^-} and m_{e^+} are the masses of the electron and positron, respectively. So the cross section per unit mass is about 10^{-4} cm^2/g. This means the self interaction of dark matter could be about four orders of magnitude stronger than the electromagnetic interaction between an electron and positron. Note that this is an average strength, as we do not know how many different dark matter particles there are, let alone how many forces it interacts with. For right now, the best we can do is examine how differing cross sections affect the development of the universe and try to match those effects with observable characteristics in order to prove that dark matter, on average, interacts with itself.

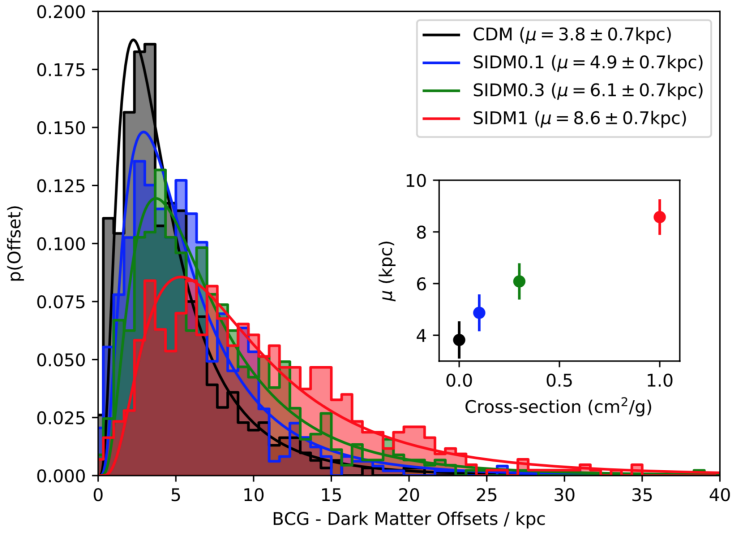

Figure 1.3: BCG offsets of SIDM models with different cross sections. As the cross section gets larger, so do the expected offsets. Graph from Harvey et al. (2019).

Kim et al. (2016) and Harvey et al. (2019) show that this average interaction can be quantified by examining how luminous matter interacts with the gravitational pull of dark matter in relaxed galaxy clusters. Once the dark matter core of a galaxy cluster is relaxed, SIDM predicts that the mass distribution of the core will be further spread out than is predicted by the original CDM model. This extended and shallower distribution will allow the BCG have larger oscillations. Figure 1.3 shows how the measured BCG offsets correspond to cross sections in simulations.

2

Methodology

Dark matter is "dark" because it does not emit, absorb, or interact with photons. Since our main tool for understanding the cosmos is collecting photons through telescopes, a direct observation of dark matter density profiles though these telescopes is impossible. Instead, we must find indirect ways of observing dark matter properties. One way to deduce the density profile of dark matter is by examining how objects around the dark matter center of mass are affected by the dark matter's gravitational field. As stated in the introduction, the object I will be examining is the BCG of each galaxy cluster.

In order to complete this analysis, I must collect a suitable sample of galaxy clusters that have high enough resolution to examine possible offsets (section 2.1). For each cluster, I need two pieces of information: first, the coordinates of its BCG (section 2.1.1), and second, the center of mass of the dark matter distribution and its associated error (section 2.2). Once we have the BCG coordinates and the center of mass of the dark matter distribution, we will be able to determine if the BCG is offset from the dark matter center of mass.

2.1 Data Collection

In order to obtain the coordinates of BCGs, I used the Dark Energy Survey (DES) year three data, one of the widest and deepest optical range surveys available (Sevilla, 2020). Specifically, I used the **red**-sequence **ma**tched-filter **P**robabilistic **Per**colation cluster finder (redMaPPer) catalog which identifies galaxy clusters and their BCGs. RedmaPPer is one of the few tools that identifies BCGs in galaxy clusters.

To analyze the x-ray data, we used data from the **M**ass **A**nalysis **T**ool for **Cha**ndra pipeline (MATCha) (Hollowood et al., 2019). MATCha analyzes archival x-ray data from the Chandra telescope, which is the source of the x-ray images I analyzed. MATCha gives us information on the cluster's R_{500} radius (defined below) and tells us whether the cluster is merging or not.

Next we had to select the best galaxy clusters to examine. The first data requirement was galaxy clusters with low redshifts.[1] We chose low redshift clusters because we want clusters that are closer, and therefore seemingly larger in the sky, to our telescopes. This higher resolution allows us to more accurately determine if the BCG is offset from the dark matter center of mass. We chose galaxies with redshifts below 0.3. We also required that the galaxies had redshifts above 0.1 because below this redshift, DES cannot identify clusters robustly.

Using these low redshift BCG coordinates from redMaPPer, we made a cut based on the signal to noise ratio of the x-ray data. We required a high signal to noise ratio because we need the lowest possible uncertainty in the x-ray measurements. A low uncertainty means the error on the dark matter center of mass will be smaller. We aim to have a very low uncertainty for our dark matter center of mass so we can accurately determine if there is an offset. Hence, we required a signal to noise minimum of 50 from the Chandra data in a 500 kilo-parsec (kpc) region.

Once we had the highest-resolution clusters possible, I required that the clusters be relaxed.

[1] In general, redshift is a good metric for defining the object's distance from us (Hubble, 1929). This is because the universe is expanding, so objects farther from us are moving away faster than object that are closer to us. Low redshift objects are closer to us, while high redshift objects are farther away from us.

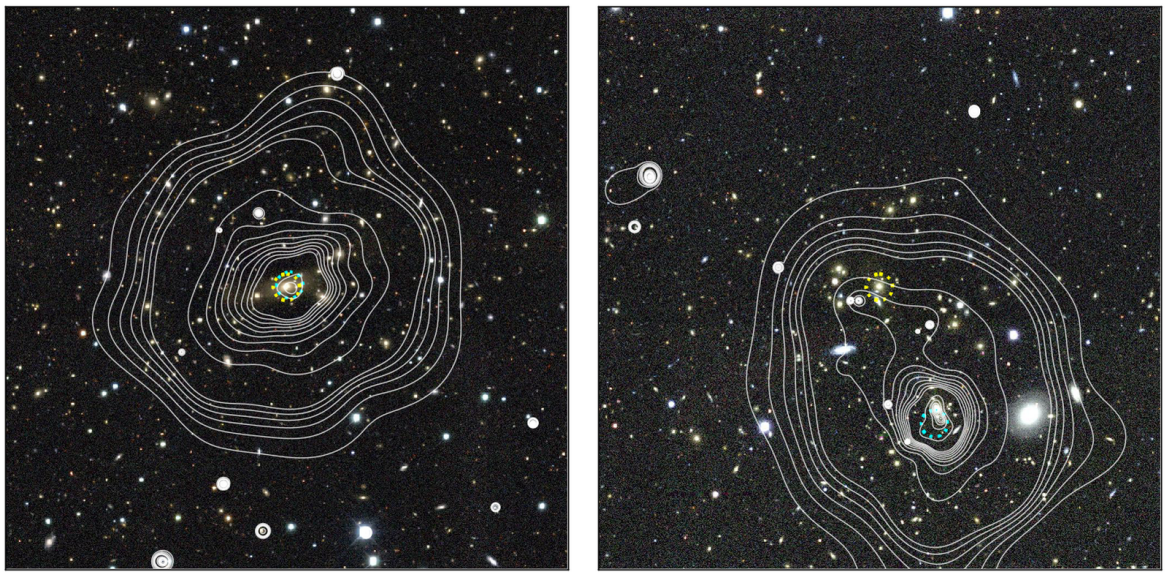

Figure 2.1: X-Ray overlays illustrating a relaxed cluster versus a merging cluster. The white lines represent contours of constant x-ray readings. The blue dotted circles represent the MATCha x-ray peak and the yellow dotted circles represent the redMaPPer BCG. The left image shows cluster 182, which is flagged as a relaxed cluster because not only are the BCG and x-ray peak close, but also the x-ray contours are roughly circular. The right image shows cluster 110, which is not a relaxed cluster because the x-ray contours are not circular. Images courtesy of Reese Wilkinson.

We require relaxed clusters because the x-ray analysis outlined in Section 2.2 only works if the luminous matter and dark matter centers of mass are aligned. In a non-relaxed cluster, the luminous and dark matter centers of mass are possibly affected by different forces. This means that the x-ray center (which corresponds to the center of mass of the ICM, or luminous matter) would not accurately represent the center of mass of the dark matter distribution, therefore rendering the BCG/x-ray offset analysis useless. The MATCha catalog identifies merging clusters, which we used to guarantee that we are examining relaxed clusters. After this final data cut, I had a sample of 14 galaxy clusters.

2.1.1 Data Verification

With these 14 clusters, we verified that the redMaPPer algorithm identified the correct BCG coordinates and that the clusters were indeed relaxed. We overlaid the x-ray data over optical images of each cluster with a mark where the BCG cluster was, as seen in Figure 2.1. We verified that each BCG was located on roughly the brightest galaxy in the cluster. Then, we verified that the identified

BCG was roughly around the center of the x-ray peak. If the initial BCG was incorrect, we marked the correct BCG and used the correct coordinates instead.

In order to verify how relaxed the cluster was, we examined the x-ray contours. We used two criteria to determine if the cluster was relaxed. First we checked if the inner contours were relatively close together and circular, as this would signify a sharp increase in the x-ray signal and a well-defined core in the center of the cluster. Next, we verified that the central contour enclosed one possible bright galaxy. If it did not, this would tell us that there was a recent merger and the BCGs of the merging galaxies hadn't relaxed to become one BCG. An example of a relaxed cluster can be seen in the leftmost panel of Figure 2.1, which has one bright galaxy at the center of the contour and the inner contours are close to each other and circular. The rightmost panel shows a non-relaxed cluster, which has many possible BCG candidates and has asymmetric x-ray contours. Once each cluster was verified or corrected, I ran them through the algorithm outlined below.

2.2 Determining the Dark Matter Center of Mass

The final part of this analysis is determining the center of mass of the dark matter distribution. As stated above, our data was collected such that each galaxy cluster in our sample has a center of mass located near the x-ray center. In order to obtain the dark matter center of mass coordinates, we must find the corresponding x-ray center.

To understand how to calculate the x-ray center, one must understand how data is collected by telescopes. Digital telescopes (like those used by DES and Chandra) collect photons through a two dimensional array of Charge Coupled Devices (CCDs). Each CCD essentially counts the number of photons coming from a small angular cutout of the sky. Once these CCDs transmit the data to a computer, the two dimensional array of CCD counts is reconstructed, making an image of the sky based on these photon counts.

This image reconstruction relies on one key point: each pixel in the two dimensional array

directly maps onto a specific Right Ascension (RA) and Declination (DEC) range.[2] Therefore, if we find the x-ray center coordinates in units of pixels, we will be able to transform those coordinates into RA and DEC.

In order to determine the centroid of a cluster image, I conducted a calculation very similar to a center of mass calculation:

$$\vec{x}_{centroid} = \frac{\sum_{i \epsilon 0.15 R_{500}} \vec{x_i} C_i}{\sum_{i \epsilon 0.15 R_{500}} C_i} \tag{2.1}$$

Where $\vec{x_i}$ is the two dimensional position vector of the i$^{\text{th}}$ pixel, and C_i is the photon count in the i$^{\text{th}}$ pixel. The pixel domain includes all of the pixels within the circle defined by 0.15 times R_{500} radius. This R_{500} radius is defined to be the radius at which the average density of the cluster is 500 times larger than the critical density of the universe.[3] The center of this circular cutout is defined to be where the x-ray peak of the image is, which acts as a first-order centroid.[4] We only accounted for pixels inside this circle for two reasons, both of which are illustrated in Figure 2.2.

First, the x-ray images from Chandra are generally not centered on the cluster. As seen in Figure 2.2, the cluster is on the bottom of the chip. If I took the centroid without using the $0.15 R_{500}$ radius, the result would be skewed towards the center of the image. Second, there are possibly other clusters or objects in the image which would skew the centroid calculation. As seen in Figure 2.2, there is a substantial x-ray source above the focused cluster. If I took the centroid without using the $0.15 R_{500}$ radius, the result would be skewed towards the other x-ray source. Accordingly, for each cluster I made a new two dimensional array which contained a circular cutout of the x-ray data with a radius that corresponds to $0.15 R_{500}$ radius and was centered on the first-order x-ray center approximation given by the MATCha catalog.[5]

[2] RA and DEC are the names of the coordinates used by astronomers. In this coordinate system, the earth's lines of latitude and longitude are projected onto the sky. The RA corresponds to the longitude and DEC corresponds to the latitude.

[3] Critical density is the density at which the current universe would have to be in order guarantee a "flat" universe. A good review on universe curvature can be found from Peebles & Ratra (2003).

[4] This x-ray peak is calculated by MATCha. It is defined to be the densest source of x-rays in the cluster that is not generated by x-ray point sources like the active active galactic nuclei in BCGs. How this peak was calculated is explained in Hollowood et al. (2019).

[5] The radius of the cutout is fifteen percent of the R_{500} radius because this is the standard galaxy cluster dark matter core size in the field of cosmology.

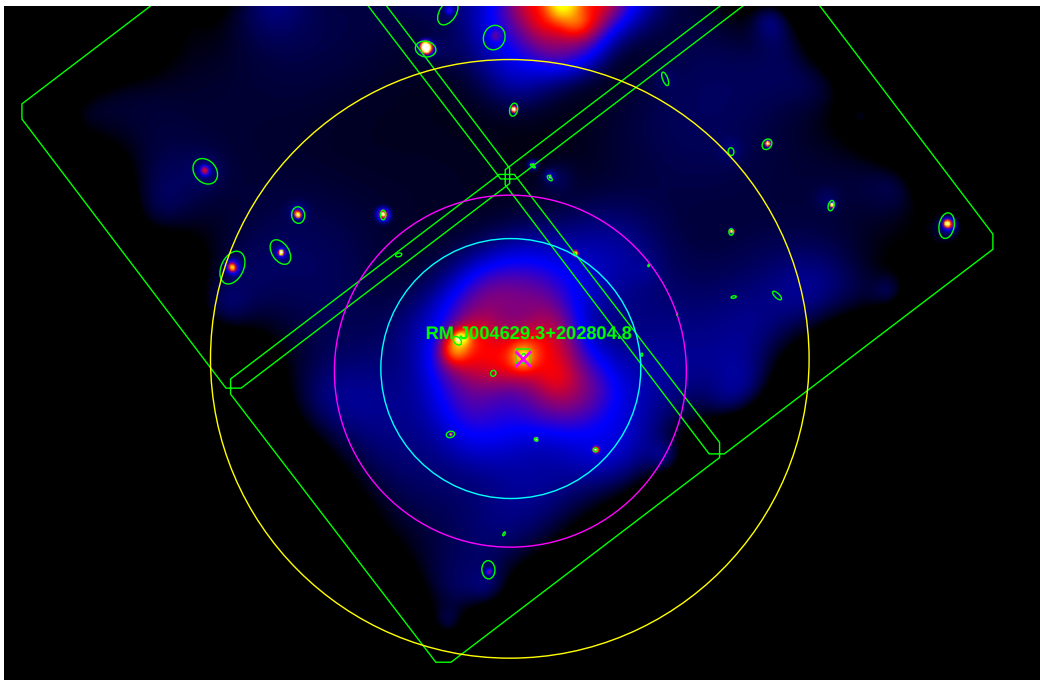

Figure 2.2: Example of X-Ray Data from DES. The cluster is not on the center of the image, and there is another large x-ray source at the top of the image. The yellow circle is the R_{500} radius. If I took the centroid of the entire image, the measurement would not accurately represent the dark matter center of mass because the measurement would be skewed to the top of this image. This is why I only took into account the pixels in the $0.15R_{500}$ radius when measuring the centroid. Courtesy of Hollowood et al. (2019).

Using Equation 2.1, I can calculate a centroid given a cutout radius, a cutout center, and a two dimensional x-ray image. A single measurement of one image per cluster will not be enough to determine the x-ray center to a suitable degree of certainty because this approach does not yet quantify how error affects these measurements. Since our data was collected by a telescope that uses CCDs to detect counts from a source, there is an associated Poisson error. I quantified the effects of this error by creating noise simulations on the data.

In each simulation I added Poisson noise to the pixels in the $0.15R_{500}$ radius, and then recalculated the centroid using Equation 2.1. For each cluster, I generated 100 noise simulations. For each simulation I calculated the distance between the BCG and the calculated x-ray center. The separation is the median distance from the BCG, and the error is the 16^{th} and 84^{th} smallest distances, which correspond to the 1-sigma errors of the measurements.

3

Results

I performed the above algorithm on the 14 original clusters. A table of the results for all of the clusters is in Table 3.1. This table shows that the median BCG offset for all clusters is larger than the upper and lower error. A visual representation of this data is seen in Figure 3.1.

Figure 3.1 shows the median offsets and their associated one sigma errors. As seen in this figure, clusters 22, 74, 100, 189, and 199 have offsets which differ from the rest by around a factor of two. These clusters will be discussed in the next chapter. This figure also shows the x-axis, or the line that represents no offset from the BCG. None of the error bars cross this line.

An example of one of these runs is shown in Figure 3.2. The first panel in this figure shows the x-ray overlay of the cluster, which has roughly circular x-ray contours. This means the cluster is relaxed. The second panel of Figure 3.2 shows an illustration of the simulation run, with the simulation centroids shown with green dots, the coordinate with the median separation marked with a blue x, and the BCG position marked with a red x. The last panel in Figure 3.2 shows a histogram of the separations, centered at around 3.25 kpc. The histogram has a roughly Gaussian shape, with the majority of centroids in the range of 2.75 to 3.75 kpc separations, with there being fewer offsets smaller or larger than this range. There were no simulated offsets below 2 kpc.

Catalog Number	Median BCG Offset (kpc)	Upper Error (kpc)	Lower Error (kpc)
1	9.163	0.979	0.673
22	51.432	0.510	0.603
74	96.662	1.181	1.229
100	60.712	0.782	1.099
159	3.185	0.281	0.386
181	30.570	0.803	0.861
182	17.074	0.699	0.686
189	78.458	1.060	0.952
199	5.929	1.106	1.047
207	16.219	0.584	0.606
438	28.244	0.615	0.538
1372	20.553	0.462	0.531
1454	7.935	0.749	0.709
1545	14.53	0.211	0.224

Table 3.1: Initial results table. For each of the clusters, the median BCG offset is larger than the upper and lower error.

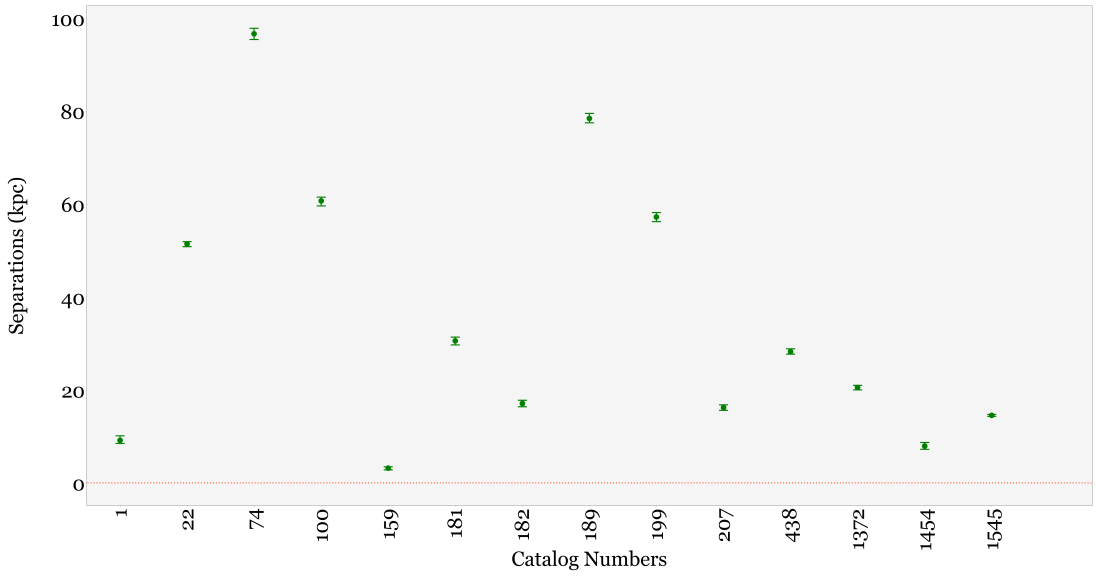

Figure 3.1: Initial results. The green marks represent the median separation calculated from the 100 simulations of each image. The upper and lower error bars represent the 84^{th} and 16^{th} smallest separations respectively. These represent the 1-sigma errors of the simulations. Clusters 22, 74, 100, 189, and 199 have unusually high offsets. These will be discussed in the next chapter.

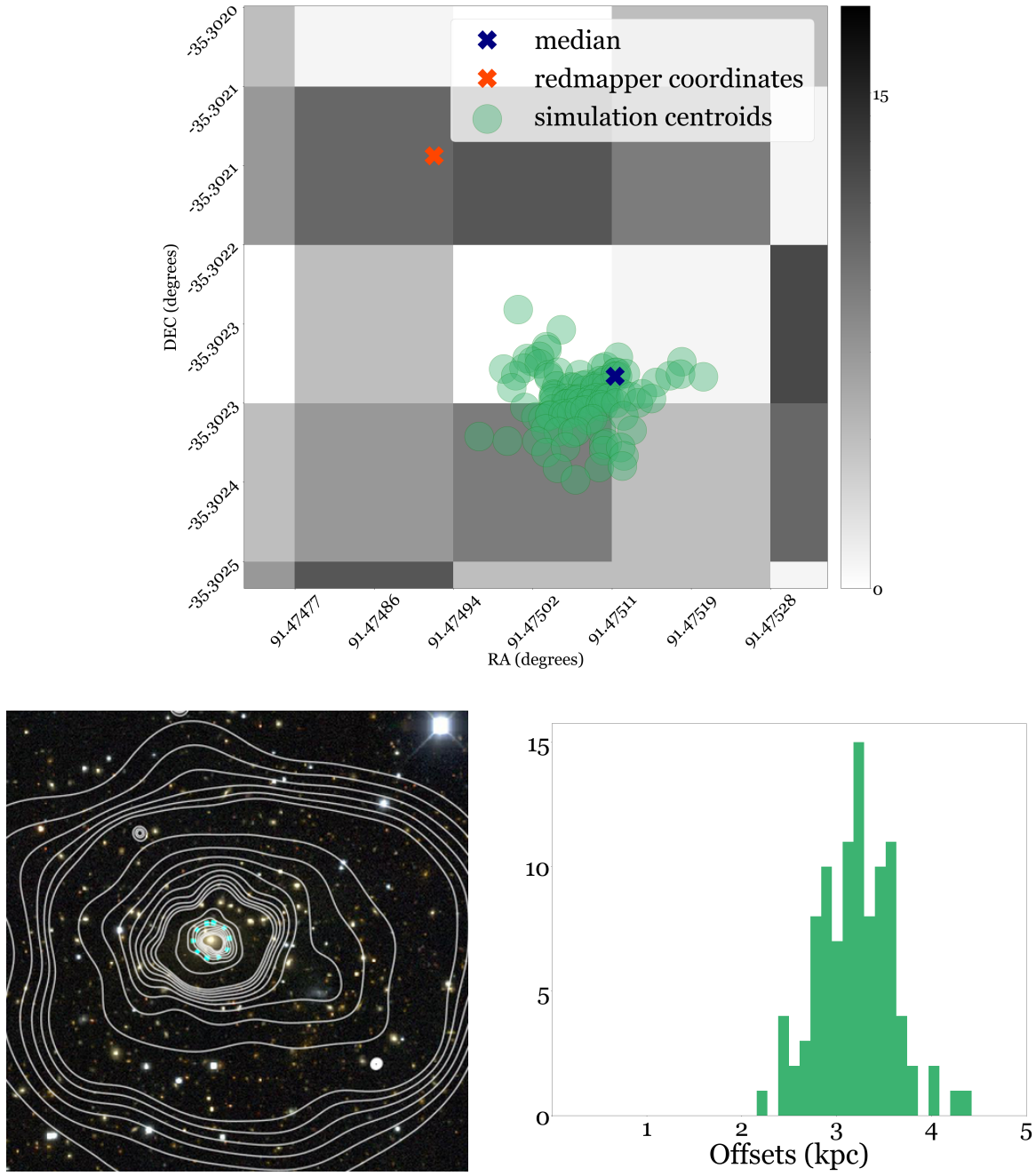

Figure 3.2: Example simulation run of cluster 159. The top panel shows the simulations centroids, marked with green dots, with the coordinate with the median separation marked with a blue x. The redMaPPer BCG coordinate is marked with a red x. Each gray box represents one pixel of the x-ray data. Each simulation centroid is less than 1 pixel from the median centroid, while the BCG is more than one pixel away from the median centroid. The bottom left panel shows the x-ray contour overlay of the optical DES image. These contours are roughly circular, meaning that this is a relaxed cluster and thus the x-ray centroid is an accurate approximation of the dark matter center of mass. The bottom right panel shows a histogram of the centroid/BCG separations. The bins have a size of around 0.1 kpc. The histogram looks roughly Gaussian, with the majority of data within about 0.5 kpc from 3 kpc separation, with few data points in the tails. X-Ray overlay courtesy of Reese Wilkinson.

4

Examining the Larger Offsets

As stated in the previous chapter, clusters 22, 74, 100, and 189 have unusually high offsets. We determined that these clusters are on the line between relaxed and merging for two reasons.

First, the x-ray profiles of these clusters are more spread out than truly relaxed clusters. The leftmost panel of Figure 4.1 illustrates this feature in cluster 22. The figure shows that the central x-ray contours are farther apart from each other than the less central contours. This means the distributions of the x-rays are relatively flat in the central region, indicating that this cluster is almost fully relaxed, but there is astrophysical disturbance of the x-ray emitting gas in the core of the cluster.

Second, there are many bright galaxies within the first few central contours of the images. As seen with cluster 22 in Figure 4.1, the BCG of this cluster was chosen to be the galaxy in the yellow circle, but there are many galaxies which are similarly bright in the central region of this image. This indicates that the clusters that merged into cluster 22 have not merged enough to where their central galaxies have combined to form one larger central galaxy. Since clusters 22, 74, 100, and 189 all exhibit these signs, it is clear that they are not completely relaxed like other clusters in this sample. However, since their overlays do not show a clear substructure of two merging clusters, we cannot exclude them from this data sample.

Figure 4.1 also shows the x-ray overlay of cluster 199. This cluster meets all of the criteria

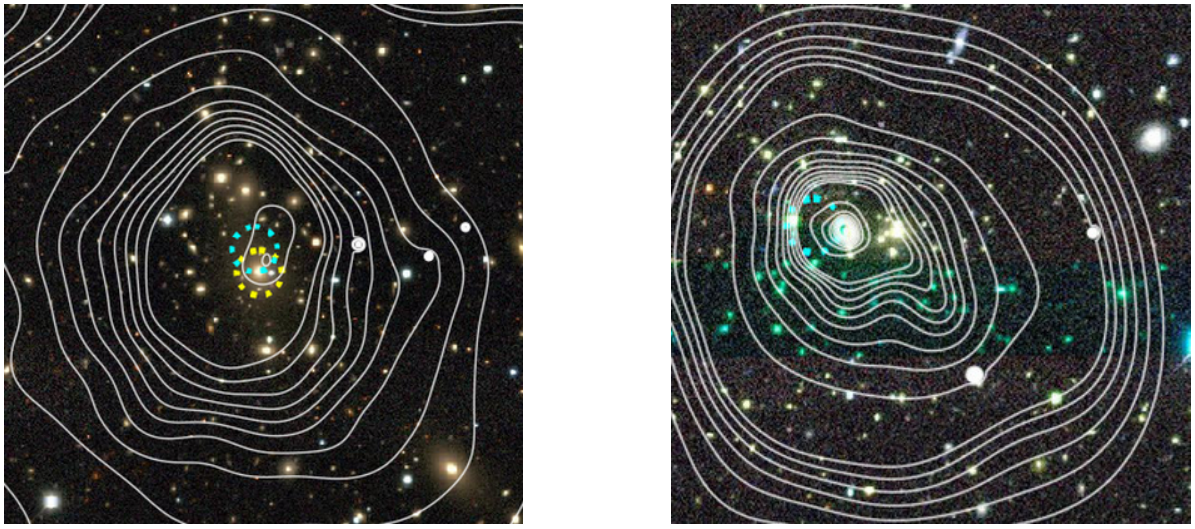

Figure 4.1: X-Ray contour overlays of optical data from clusters 22 and 199. The white lines in each image show lines of constant x-ray readings. The left image is of cluster 22, which has a very shallow x-ray profile and multiple possible BCGs. This cluster is not clearly a relaxed cluster, but it is also not clearly a merging cluster, so we must include it in our data. I found similar results for clusters 74, 100, and 189. The right image is cluster 199, which has relatively circular contours and a clear central x-ray peak. Thus, cluster 199 is a relaxed cluster. Despite this relaxed signature, the calculated BCG/x-ray center offset is large, as seen in Figure 3.1. Figure 4.2 illustrates why the calculated offset is so large. Images courtesy of Reese Wilkinson.

for a relaxed cluster, but still has an unusually high offset. Figure 4.2 shows the x-ray signature of the cluster. The diamond, which marks the simulation with the median distance from the BCG, is halfway between the BCG (marked by a red circle) and the first order x-ray center (marked by a red x). The x-ray counts in Figure 4.2 are much denser around the BCG coordinates than they are around the first-order x-ray center. This indicates that the MATCha algorithm recognized the wrong x-ray peak. This could have happened because the x-ray profile is very sharp, as seen in Figure 4.1. Since the profile is so sharp, the algorithm recognized the peak as a point source and removed it from consideration as the x-ray peak. Thus, it chose the next best spot.

The algorithm outlined in the previous chapter assumes that the x-ray peak is a good approximation of the x-ray center. A miscalculation in the first-order x-ray center affects the offset measurement because the x-ray peak determines the center of the $0.15R_{500}$ radius cutout I used to calculate the centroid. The first-order centroid is not a reasonable center for the circular cutout for cluster 199, and thus rather than making a second-order correction to the first order approximation,

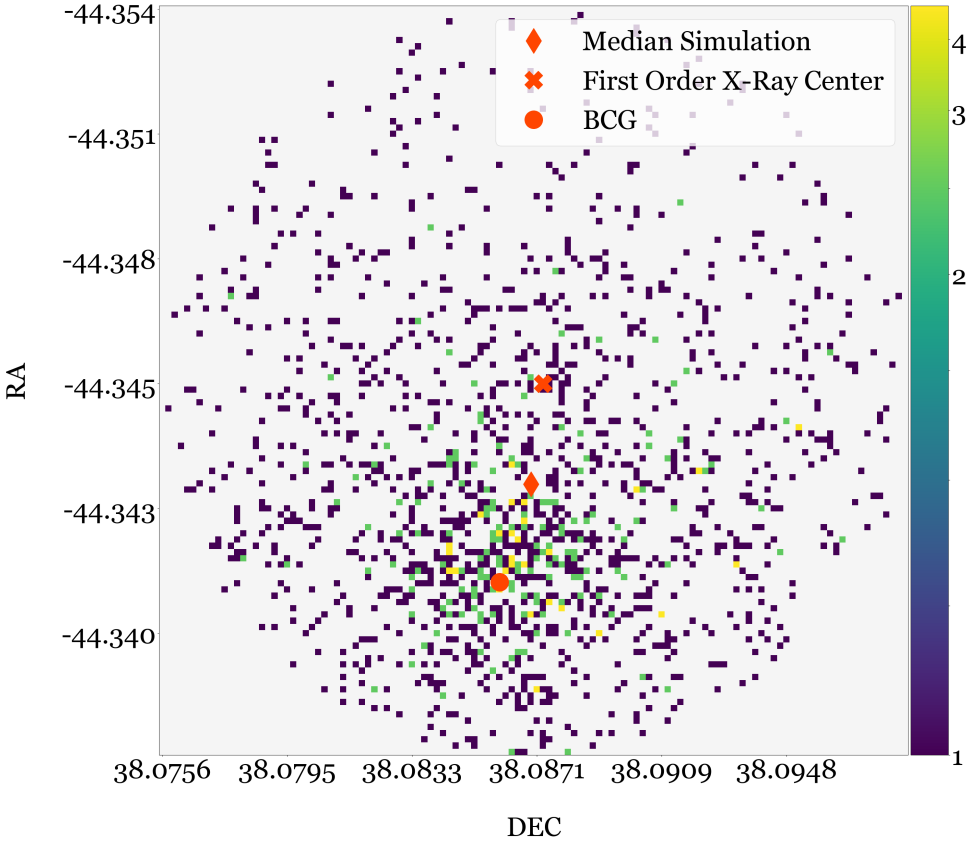

Figure 4.2: Simulations of cluster 199. The image represents the x-ray data from Chandra within the $0.15R_{500}$ radius. The color bar on the right indicates the color the corresponds to 1, 2, 3, and 4 counts detected from Chandra. The red x represents the first-order x-ray center from the MATCha catalog, the red circle represents the BCG coordinate, and the red diamond represents the calculated centroid. The first order x-ray center determines how the algorithm cuts the data into a circle. While the calculated centroid is technically correct given the algorithm, it clearly misrepresents the actual x-ray center, which should be closer to the center of the data patch with high photon counts, closer to the BCG. This shows that for this cluster I needed to use a different first-order approximation for the x-ray center.

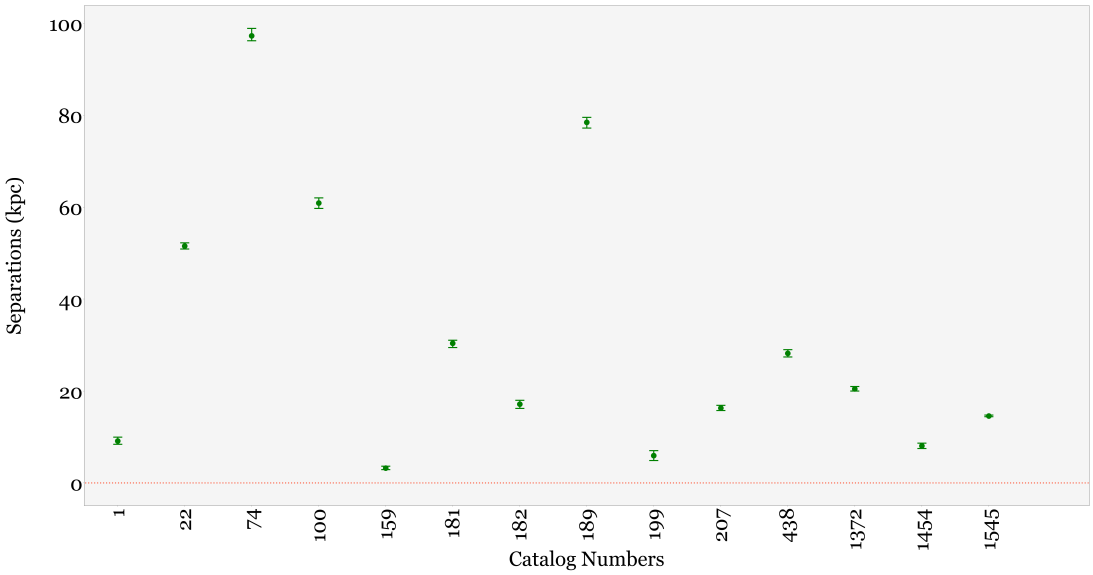

Figure 4.3: Calculated offsets of the final 14 clusters and their errors. The upper and lower error bars represent the 84^{th} and 16^{th} percentile separations respectively. The orange dotted line is the x-axis.

the algorithm found a centroid which is half-way in between the actual x-ray center and the incorrect x-ray peak, as shown in Figure 4.2. While the algorithm outlined in the previous chapter did technically give the correct centroid of this two dimensional array, the calculation does not correctly represent the actual x-ray centroid for the cluster.

In order to get an accurate reading of the x-ray center, I had to use a different estimated x-ray peak for the $0.15R_{500}$ cutout. For this cluster, the BCG is roughly near the x-ray peak, so I used the BCG's coordinates as the first-order estimation of the x-ray center. The final results are illustrated in Figure 4.3. In this final graph, the dots represent the median separation measurement and the error bars represent the 1σ error in the x-ray measurement. Each data point has a median separation measurement which is at minimum 3σ from zero.

The spatial resolution of the Chandra x-ray telescope is 0.492 arc-seconds, which translates to between 1.14 and 3.81 kpc for a redshift range of 0.1 to 0.3. This means that the smallest measured offsets are larger than one pixel, and thus the resolution of the Chandra data is high enough to ensure that these results are statistically significant.

5

Discussion

The data from Figure 4.3 shows that the BCG/x-ray center offsets are larger than zero to more than a 1-sigma degree of certainty. This supports the SIDM model.

In order to better constrain the self-interaction cross section of dark matter, we look to Figure 1.3, which shows how the distributions of BCG offsets would differ with different cross sections. Figure 5.1 shows the histogram of the measured offsets. I fit a log-normal curve to the points on the histogram and found that the best fit offset is 12.30 $\pm$ 0.72 kpc. This fit includes the clusters which are on the border between relaxed and not relaxed. Harvey et al. (2019) places very strict guidelines on the relaxation of clusters, so the outlying clusters (22, 74, 100, and 189) would not be considered for the fit in Figure 1.3. If the outlying clusters are removed as in Harvey et al. (2019), then the best fit offset is 10.18 $\pm$ 1.77 kpc.

These median offsets are much smaller than the offsets predicted by the simulations from Kim et al. (2016). This inconsistency is expected because these simulations were dark matter only, and thus can only roughly predict what the offsets would look like for a universe with dark and luminous matter. On the other hand, compared to Harvey et al. (2019), these results are within the one sigma error for the currently accepted SIDM upper-limit cross section of 1 cm^2/g, and they're within two sigma error for a low cross section of 0.3 cm^2/g. In order to completely understand these results, it is important

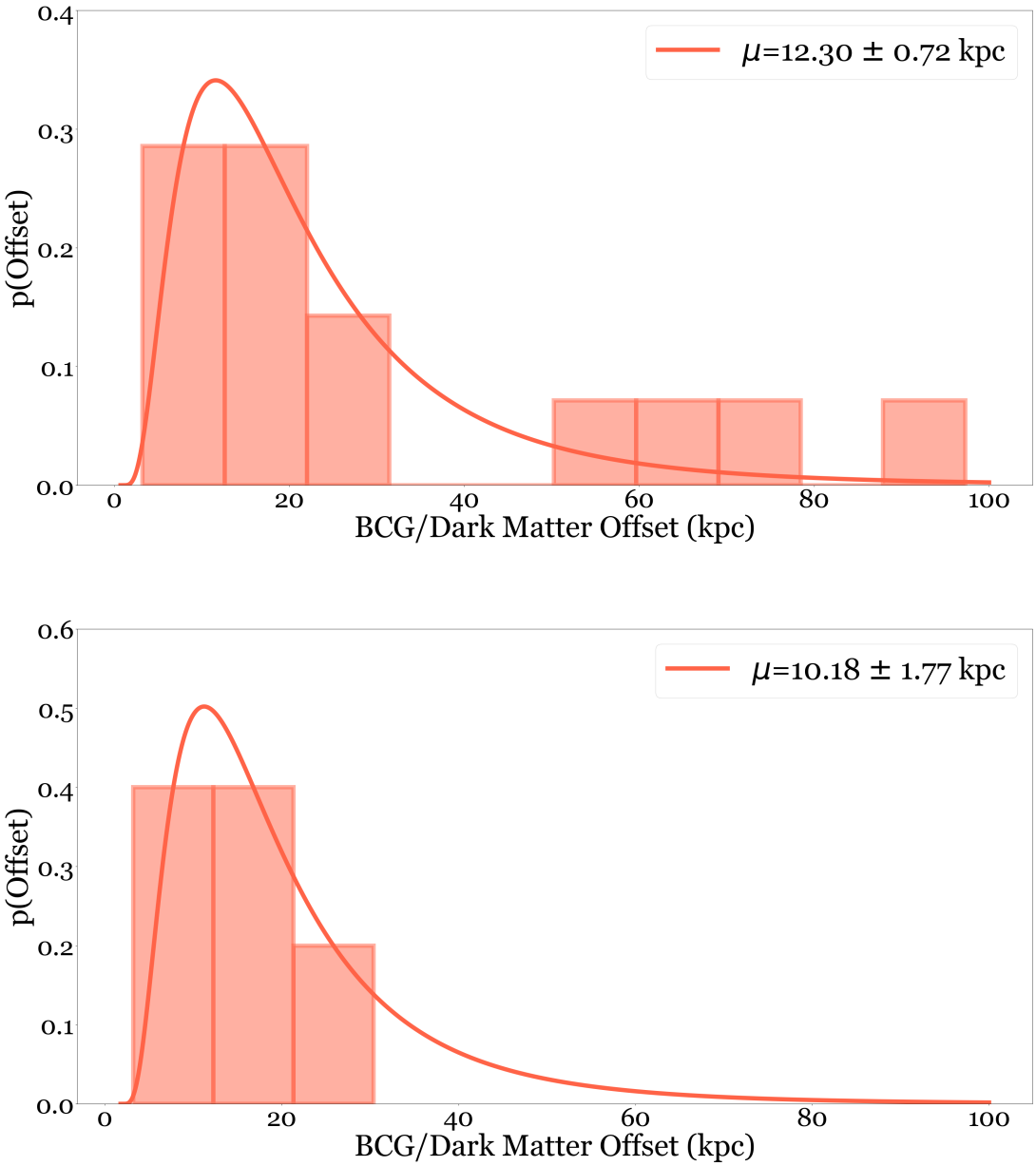

Figure 5.1: Histograms of the calculated offsets. The top panel shows all of the calculated offsets from the original 14 clusters. I fit a log-normal function to the data. The best fit offset is 12.30 ± 0.72 kpc for the 14 clusters. The outlying cluster offsets imply that those clusters would not be considered "relaxed" by Harvey et al. (2019), so the second panel shows a fitted curve to just the offsets within 40 kpc. The best fit offset for these clusters is 10.18 ± 1.77 kpc.

to understand the limits of these comparisons.

One limitation is the simulations I am comparing with my results. In order to simulate the formation of large-scale structure, Harvey et al. (2019) used baryonic physics that has been developed over the past 20 years, and is still being perfected today. Since the results in this thesis are very sensitive to the accuracy of these simulations, a change to the simulation engine used in Harvey et al. (2019) could lead to a different interpretation of the results presented above.

Furthermore, the x-ray signatures of these dark matter cores are an indirect method of detecting dark matter. This means we are inferring that the dark matter is in the same place as the x-ray emitting gas. However, we cannot be sure that these x-ray centers actually reflect the dark matter centers of mass to the precision that we are measuring. Gravity works on large timescales, so while the x-ray gas might look relaxed, the underlying dark matter could be in a less relaxed state, or have a completely different structure from what we are assuming.

5.1 Next Steps

The current sample of 14 clusters (of which 10 were fully relaxed by the standards of Harvey et al. (2019)) could be increased with a few changes to the data collection. First, I could use an optical survey with more low-redshift galaxy clusters, such as the Sloan Digital Sky Survey (SDSS). This could give us more clusters to examine. Second, we could also make the signal to noise cut smaller. The errors determined from the clusters with a signal to noise of higher than 50 were very small compared to the offsets. If I used a lower signal to noise cut, then the results would most likely still be significant enough to determine if there is an offset.

Furthermore, in order to avoid issues like cluster 199 and have a more uniform approach to finding the true x-ray center, I could create a convergence algorithm. This would mean finding the x-ray centers like I did before, then taking that center and creating a new $0.15R_{500}$ cutout, taking the centroid again, and testing if the two centroids are consistent with each other. If they are not, then

continue to make the new $0.15R_{500}$ cutouts until the x-ray centers converge to the same coordinates.

If I increase the number of possible galaxy cluster candidates, make the signal to noise cut smaller, and create a convergence algorithm to determine the x-ray peak, then the results would be even more statistically significant and accurate.

5.2 Conclusion

The BCG/x-ray center offsets are significantly larger than zero. These results are consistent with dark matter self interaction. With the improvement of simulation techniques and a larger cluster sample size, we can possibly decrease the upper limit to the dark matter self-interaction cross section. This result gives us a glimpse into what dark matter is and how it interacts with itself. Since these BCG/x-ray offsets exist, it is possible that large-scale dark matter masses have a flatter density distribution than is predicted by CDM. This means that future dark matter models might have to incorporate more complex force interactions than simple interaction through gravity.

Bibliography

Anderson, L., Aubourg, E., Bailey, S., Beutler, F., Bhardwaj, V., Blanton, M., Bolton, A. S., & Brinkmann, J. (2014). The clustering of galaxies in the sdss-iii baryon oscillation spectroscopic survey: baryon acoustic oscillations in the data releases 10 and 11 galaxy samples. *Monthly Notices of the Royal Astronomical Society*, Volume 441, 24–62.

Carlson, E. D., Machacek, M. E., & Hall, L. J. (1992). Self-interacting dark matter. *Astrophysical Journal*, 398.

Casertano, S. & van Gorkom, J. H. (1991). Declining rotation curves: The end of a conspiracy? *The Astrophysical Journal*, 101, 1231–1241.

Davis, M., Efstathiou, G., Frenk, C. S., & White, S. D. M. (1985). The evolution of large-scale structure in a universe dominated by cold dark matter. *The Astrophysical Journal*, 292, 371–394.

de la Torre, S., Guzzo, L., Peacock, J. A., Branchini, E., Iovino, A., Granett, B. R., Abbas, U., & Adami, C. (2013). The vimos public extragalactic redshift survey (vipers) . galaxy clustering and redshift-space distortions at z $\approx$ 0.8 in the first data release. *Astronomy and Astrophysics*, 557.

Delliou, M. L., Marcondes, R. J. F., & Neto, G. B. L. (2019). New observational constraints on interacting dark energy using galaxy clusters virial equilibrium states. *Monthly Notices of the Royal Astronomical Society*, 490, 1944–1952.

Dubinski, J. & Carlberg, R. G. (1991). The structure of cold dark matter halos. *Astrophysical Journal*, 378, 496.

Faber, S. M. & Gallagher, J. S. (1979). Masses and mass-to-light ratios of galaxies. *Annual Review of Astronomy and Astrophysics*, 17, 135–187.

Flores, R., Primack, J. R., Blumenthal, G. R., & Faber, S. M. (1993). Rotation curves from baryonic infall: Dependence on disk-to-halo ratio, initial angular momentum, and core radius, and comparison with data. *Astrophysical Journal*, 412, 443–454.

Flores, R. A. & Primack, J. R. (1994). Observational and theoretical constraints on singular dark matter halos. *Astrophysical Journal Letters*, 427, L1–L4.

Gordon & Breach (1967). The total cross section in e^+ and e^- annihilation and the new particles. In *Comments on Nuclear and Particle Physics*. Gordon and Breach.

Gott, J. R., I. & Rees, M. J. (1975). A theory of galaxy formation and clustering. *Astronomy and Astrophysics*, 45, 365–376.

Harvey, D., Robertson, A., Massey, R., & McCarthy, I. G. (2019). Observable tests of self-interacting dark matter in galaxy clusters: Bcg wobbles in a constant density core. *Monthly Notices of the Royal Astronomical Society*, 488.

Hollowood, D. L., Jeltema, T., Chen, X., Farahi, A., Evrard, A., Everett, S., Rozo, E., Rykoff, E., Bernstein, R., Bermeo-Hernandez, A., Eiger, L., Giles, P., Israel, H., Michel, R., Noorali, R., Romer, A. K., Rooney, P., & Splettstoesser, M. (2019). Chandra follow-up of the sdss dr8 redmapper catalog using the matcha pipeline. *The Astrophysical Journal Supplement Series*, 244.

Hubble, E. (1929). A relation between distance and radial velocity among extra-galactic nebulae. *Proceedings of the National Academy of Sciences*, 15(3), 168–173.

Kim, S., Peter, A., & Wittman, D. (2016). In the wake of dark giants: New signatures of dark matter self interactions in equal mass mergers of galaxy clusters. *Monthly Notices of the Royal Astronomical Society*, 469.

Lin, Y.-T. & Mohr, J. J. (2004). K-band properties of galaxy clusters and groups: Brightest cluster galaxies and intracluster light. *The Astrophysical Journal*, Volume 617, 879–895.

Markevitch, M., Gonzalez, A. H., Clowe, D., Vikhlinin, A., Forman, W., Jones, C., Murray, S., & Tucker, W. (2004). Direct constraints on the dark matter self-interaction cross section from the merging galaxy cluster 1e 0657-56. *The Astrophysical Journal*, 606, 819–824.

Martin, J., Ringeval, C., & Vennin, V. (2013). Encyclopædia inflationaris. *Physics of the Dark Universe*, 5, 75–235.

NASA & WMAP (2012). Nine year microwave sky.

Peebles, P. J. & Ratra, B. (2003). The cosmological constant and dark energy. *Reviews of Modern Physics*, 75, 559–606.

Percival, W. J., Baugh, C. M., Bland-Hawthorn, J., Bridges, T., Cannon, R., & Cole, S. (2001). The 2df galaxy redshift survey: the power spectrum and the matter content of the universe. *Monthly Notices of the Royal Astronomical Society*, 327, 1297–1306.

Perkins, D. (2009). The expanding universe. In *Particle Astrophysics* chapter 2. Oxford University Press.

Read, J. I., Goerdt, T., Moore, B., Pontzen, A. P., Stadel, J., & Lake, G. (2006). Dynamical friction in constant density cores: a failure of the chandrasekhar formula. *Monthly Notices of the Royal Astronomical Society*, 373, 1451–1460.

Rubin, V. C. & Ford, W. K. (1970). Rotation of the andromeda nebula from a spectroscopic survey of emission regions. *Astrophysical Journal*, 159, 379.

Sevilla, N. (2020). in preparation.

Spergel, D. N. & Steinhardt, P. J. (2000). Observational evidence for self-interacting cold dark matter. *Physical Review Letters*, 84, 3760–3763.

Springel, V., White, S. D. M., & A Jenkins, e. a. (2005). Simulations of the formation, evolution and clustering of galaxies and quasars. *Nature*, 435, 629–636.

White, M., Scott, D., & Silk, J. (1994). Anisotropies in the cosmic microwave background. *Annual Review of Astronomy and Astrophysics*, 32, 319–370.

Yang, J., Turner, M. S., Steigman, G., Schramm, D. N., & Olive, K. A. (1984). Primordial nucleosynthesis : a critical comparison of theory and observation. *Astrophysical Journal*, 281, 493–511.

Zwicky, F. (1933). Die rotverschiebung von extragalaktischen nebeln. *Helvetica Physica Acta*, 6, 110–127.